PARTIAL LEADING EDGE FORCING OF A DELTA WING AT HIGH ANGLES OF ATTACK

Stefan Siegel*, Thomas E. McLaughlin†, and Julie A. Albertson‡

Department of Aeronautics
US Air Force Academy, CO 80840-6222

Abstract

Wind and water tunnel measurements investigating periodic forcing along sections of the leading edge of a 70° delta wing were conducted. Previous research had shown that forcing along the entire leading edge is effective in increasing lift and delaying stall. The current investigations compare forcing along the front half, rear half and entire leading edge with no forcing at all. All investigations were conducted at a nondimensional frequency F+ of 1.75 and a momentum coefficient of 0.004.

The wind tunnel investigations were used to determine the effect of forcing the flow along parts of the leading edge on the normal force. They show that forcing is most effective along the rear portion of the delta wing leading edge, downstream of vortex breakdown. At 35° angle of attack an increase in normal force coefficient of about 25% was achieved using either the entire leading edge or the rear portion only, while the front portion forcing showed only minor improvement. PIV measurements in a low speed water tunnel revealed that this increase is due to a shear layer vortex carrying high momentum fluid into the wake downstream of the vortex breakdown. Since the shear layer vortex only reaches the wake in the entire leading edge and rear half of the leading edge cases, the front half forcing does not show this normal force increase.

Nomenclature

B Local Wing Span

C Wing root chord

C_μ $=2(H/C)(\langle u'\rangle/U_\infty)^2$, Oscillatory momentum coefficient

f Frequency

F^+ $(f\,C)/U_\infty$, Nondimensional frequency

$\langle u'\rangle$ R.M.S. amplitude of velocity fluctuations

U_∞ Freestream velocity

X,Y,Z Cartesian coordinates fixed with the wing. Origin at the wing apex, X axis is aligned with the root chord line.

U,V,W Velocity components of the flow in the X,Y,Z directions.

α Wing angle of attack

Introduction

The need to improve fighter aircraft and missile maneuverability has inspired extensive study of the flow past delta wings and of methods to delay vortex breakdown. In recent years, the efficacy of oscillatory flow excitation with zero net mass flux and non-zero momentum flux has been shown[2-10]. It is more effective for delay-

---

* Postdoctoral Researcher, Department for Aeronautics, Member

† Research Associate, Department for Aeronautics, Associate Fellow

‡ Associate Proffesor Department for Aeronautics, Associate Fellow

ing separation from a lifting surface or promoting reattachment of initially separated flow, relative to steady blowing traditionally used for this purpose. This concept has been proven for a delta wing[2-3], some basic configurations[5,6], airfoils[7] and a swept-back configuration[8].

Guy et al[2] conducted a preliminary wind tunnel investigation and reported that periodic blowing and suction delays vortex breakdown and increases the local velocity over a 70° delta wing after the onset of vortex breakdown. The increased velocity indicates a decrease of the local pressure; hence an increase of the lift force can be anticipated at angles of attack where vortex breakdown exists without flow excitation. Based on time averaged LDV velocity measurements and oil flow visualization, they concluded that periodic blowing and suction, applied at the leading edge of a delta wing, increases lift and delays vortex breakdown by approximately 0.35 chord length at 35° angle of attack.

Following these encouraging results, Guy et al[3] found that the periodic flow excitation delays wing stall and greatly increases the normal force at angles of attack where stall would have occurred otherwise. At a constant oscillatory momentum coefficient, the effect of the flow excitation is maximized at a non-dimensional frequency (F+) of 1.75. At a constant frequency, an almost asymptotic increase of the normal force is observed as the momentum coefficient increases. The effect of the periodic flow excitation reaches its maximum at a momentum coefficient (c_μ) of 0.004 approximately. These results are consistent with results that were obtained in previous investigations. A maximum increase of 38% in the normal force was obtained at an angle of attack of 40° at these test conditions, relative to the unforced case. A 10° delay of the stall angle was achieved.

Despite these encouraging results, the nature of the mechanism by which periodic blowing and suction couples to and interacts with the primary delta wing vortex had been elusive up to that point. Recently, Siegel et al [1] demonstrated that the two main vortices that dominate the unforced flow field are stationary without forcing. With forcing, however, the vortex centers travel both in spanwise and wing normal directions along an elliptic path. The streamwise vortex breakdown location was found unchanged as determined by measurements of the streamwise vorticity component. Instead, the forcing increased the axial velocity in the line of the vortex core downstream of the vortex breakdown location, thus decreasing the local surface pressure and increasing normal force. This effect was attributed to the formation of a shear layer vortex during the blowing cycle, which carried high momentum fluid into the wake left downstream of the main vortex breakdown. The wake was weakened in synchronization with the presence of the shear layer vortex through the forcing cycle.

These findings suggest that the main benefit from forcing is obtained by entraining high momentum fluid from the mean flow into the wake left downstream of vortex breakdown. Therefore, if only the area downstream of the vortex breakdown is forced, the benefits of forcing the flow should be similar to the case investigated by Siegel et. al., where the entire length of the leading edge was used.

This paper outlines the results of a particle image velocimetry (PIV) and pressure tap study at the USAF Academy, wherein flow behavior on the suction side of a 70° delta wing is studied throughout the blowing/suction oscillation cycle. Alternating blowing and suction is applied to sections of the leading edge, comparing it both to no forcing and entire leading edge forcing. Through this effort, time histories of the velocity flow field illustrate flow behavior and the mechanism of lift increase in the presence of this type of flow control.

Experimental Setup

Wind Tunnel

The setup used for the wind tunnel measurements is the same as described in Reference 3. The facility used is the US Air Force Academy Low Speed Open Loop Wind Tunnel. Its test section is 910mm by 910mm in cross section and 2.5 m long. Over a velocity range up to 30 m/s the turbulence level is less than 0.2%. For the current investigations the tunnel was operated at a free stream velocity of 4.3 m/s resulting in a chord Reynolds number of 2.1×10^5.

The model employed was a flat plate semi span delta wing model of 70° sweep with a 25° bevel on the windward side. The model had 740 mm chord length and a 3 mm wide blowing and suction slot along the leading edge. For the current investigation this leading edge slot could be partially closed. Blowing and suction was performed using an externally mounted loud speaker connected to the leading edge through a duct. It was operated at a frequency of 10 Hz for the current investigations, resulting in a nondimensional frequency F+ of 1.7. The momentum coefficient was $C\mu = 0.004$. An array of pressure ports on the suction side of the model

was used to determine the normal force coefficient. For details of the setup refer to Reference 3.

Water Tunnel

A flat-plate delta wing with a leading-edge sweep of 70° and a 25° bevel on the lower surface, was investigated in the USAF Academy 38 cm x 110 cm free-surface water tunnel. The wing was sting-mounted and placed inverted at an angle of attack of 35 degrees in the water tunnel.

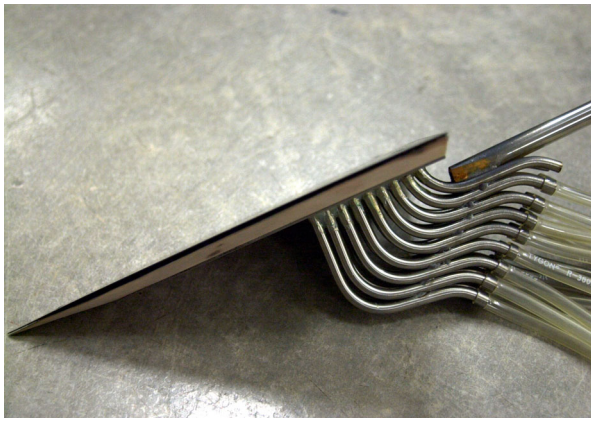

FIGURE 1. Water tunnel delta wing model

The wing has a chord length of 270 mm, is hollow and has a 2.5 mm wide slot along its leading edge. The blowing and suction slot is internally segmented into 9 individually connected channels for each side, each 10 percent of the leading edge in length starting at 10 percent of the leading edge length from the tip. These channels connect to 1/4" diameter tygon tubing as shown in Figure 1.

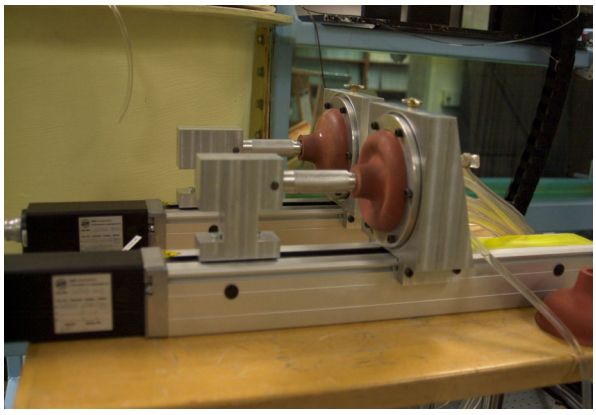

FIGURE 2. Water tunnel blowing and suction actuators

Outside of the water, the tubing leading to each leading edge segment can be connected to either one of two blowing and suction actuators as shown in Figure 2. These actuators consist of rubber bellows that can be compressed by a linear traverse slide, which is driven by a stepper motor. By compressing or expanding the bellows, water inside the bellows is pushed into or sucked out of the connected tubing, thus accomplishing blowing and suction at the leading edge of the model. The stepper motor position is controlled by a National Instruments motion control board, type PCI-7344.

For the scope of the current investigation, the blowing and suction slots were connected to the actuators in a fashion that allowed for three different blowing and suction configurations. In the configuration "Front", the leading edge starting at 20% of the chord up to but not including 60% chord was actuated. The configuration "Rear" involved actuation from 60% chord up to the trailing edge. In the configuration "Entire Leading Edge" the blowing and suction slots starting at 20% chord up to the trailing edge were used for forcing. The momentum coefficient was kept constant at a (c_μ) of 0.004, the forcing frequency at a F+ of 1.7. These settings matched the wind tunnel experiments.

Measurement Technique, Data Acquisition and Post Processing

To sample the flow, a two-component self designed PIV system implemented in LabVIEW operating a New Wave *Gemini* 125 mJ Nd:Yag laser operating at 532 nm was used. A Kodak *Megaplus* ES 1.0 CCD camera (1000 x 1000 pixel resolution) was mounted downstream of the delta wing, to visualize the flow in a plane perpendicular to the model suction surface (Figure 3). A special plexiglass viewing box was used to facilitate viewing of planes perpendicular to the wing, avoiding the inherent refraction from the water surface. For measurements in a plane at a constant spanwise location, the laser was set up below the test section illuminating the flow from below, while the camera imaged the flow through the side window.

The operating parameters for the PIV system were kept constant throughout the study. Seeding was provided using 20 μm Polyethylene particles. The system operated in cross correlation mode using two images, which were correlated directly. A 32x32 pixel interrogation

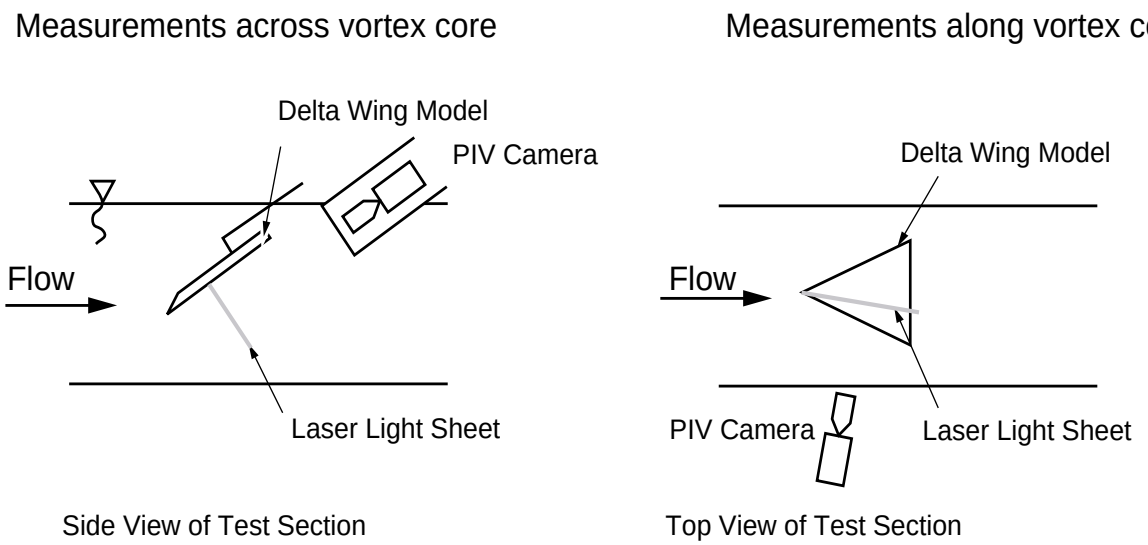

FIGURE 3. Setup of PIV system

area was used, and the images were processed with 50 % overlap yielding a raw vector field of 50 x 50 vectors.

PIV images were phase-referenced to the forcing mechanism, to allow phase averaging of 25 images, thus increasing signal-to-noise ratio of the data. Data sets were obtained every ten degrees through the 360° forcing cycle. Basic data reduction was done using self written algorithms in *Matlab* for vector validation, spatial moving average smoothing in a 3 x 3 vector area and averaging of the 25 data sets.

Results and Discussion

In the wind tunnel experiments, the effect of forcing the flow along the front half of the leading edge versus the rear half is shown in Figure 4. While the normal force coefficient of the rear half forcing case is close to the effect of forcing along the entire length of the leading edge, the front half forcing case is very similar to the unforced case. Only for angles of attack of 36° and higher does the normal force coefficient in this case significantly exceed the unforced case.

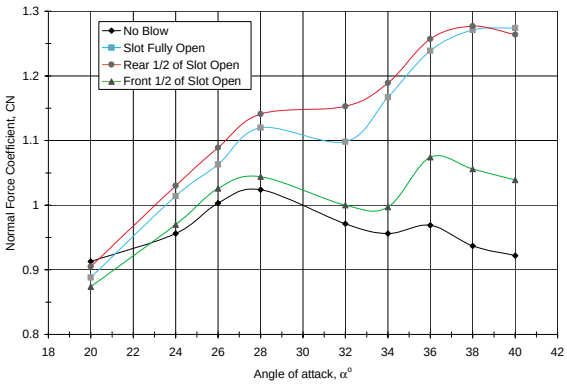

FIGURE 4. Normal force comparison of front half versus rear half of leading edge forcing

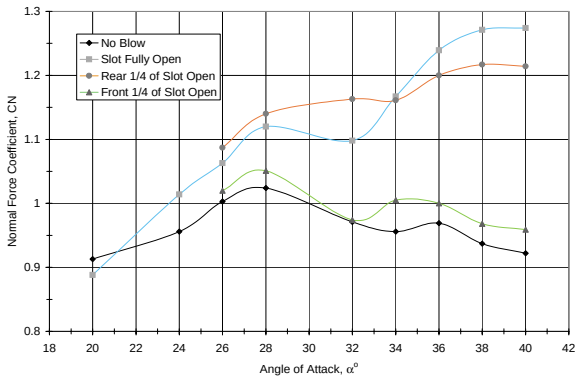

FIGURE 5. Normal force comparison of front quarter versus rear quarter of leading edge forcing

If only one fourth of the length of the blowing and suction slot is used for forcing, the results are similar to the one half length forcing case discussed above, see Figure 5. For forcing the front quarter, no significant improvement in normal force can be observed throughout the entire angle of attack range.

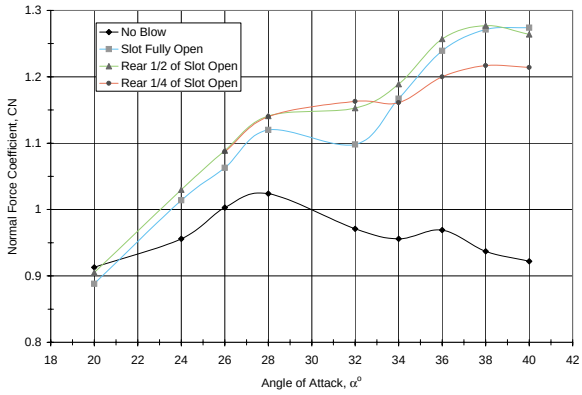

FIGURE 6. Normal force comparison of front quarter versus rear half of leading edge forcing

Comparing forcing the rear half versus the rear quarter of the blowing and suction slot, Figure 6 shows that only for angles of attack of 34° and higher a benefit of the longer forcing length can be observed.

Figures 7 and 8 show the vorticity plots normalized by freestream velocity and root chord, derived from PIV measurements in the water tunnel. Plots indicate vorticity derived from velocity measurements in a plane perpendicular to the model surface. Figure 7 displays the vorticity field at 40% of root chord location over the entire semispan, at 60° in the forcing cycle (maximum blowing velocity is at 90°). The top left graph indicates the baseline case with no suction, with forcing along the entire leading edge to the right. The bottom left and right plots show the front only and rear only forcing cases. Unforced, the primary vortex is centered at approximately 60% of the semispan, at 40% height, and

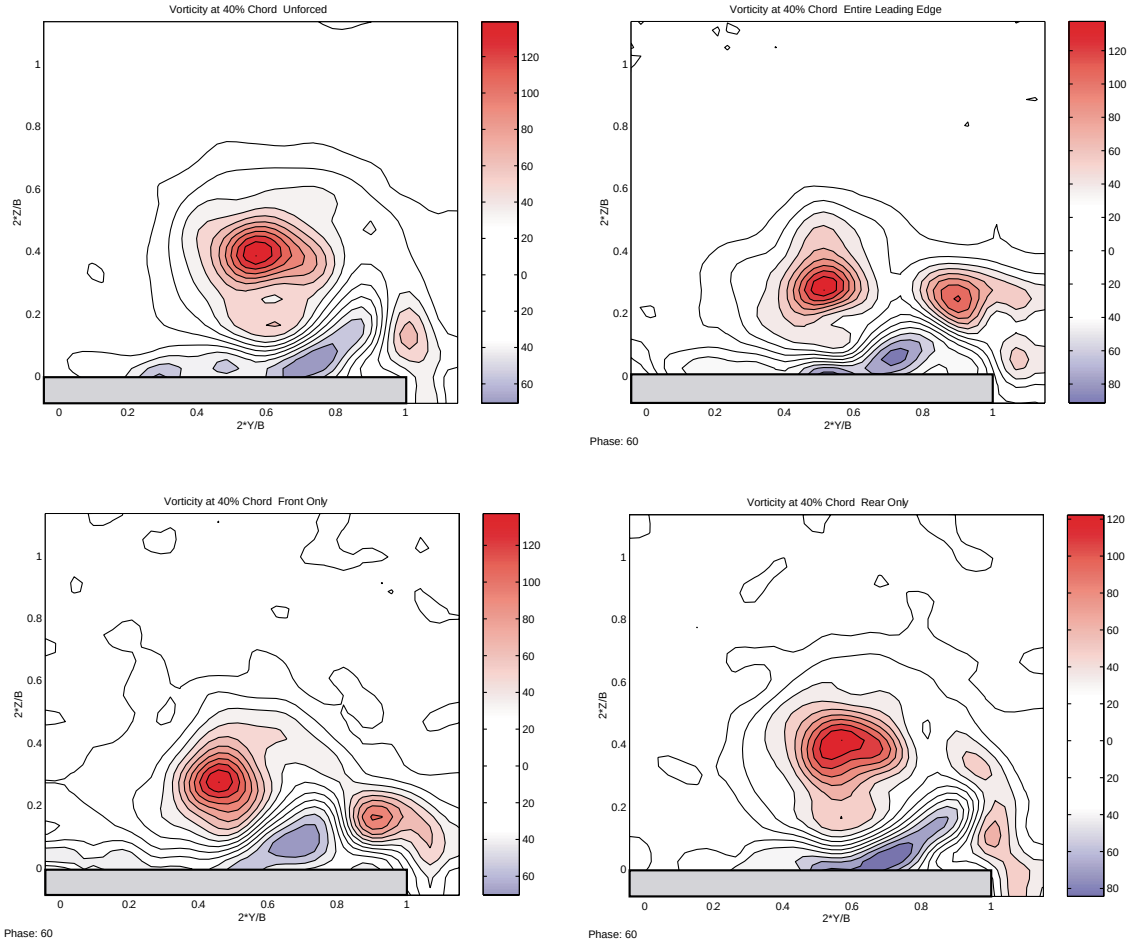

FIGURE 7. Vorticity at 40% of the root chord for the unforced, entire leading edge, front and rear only cases. All forced cases are shown at 60 degrees phase of the forcing cycle

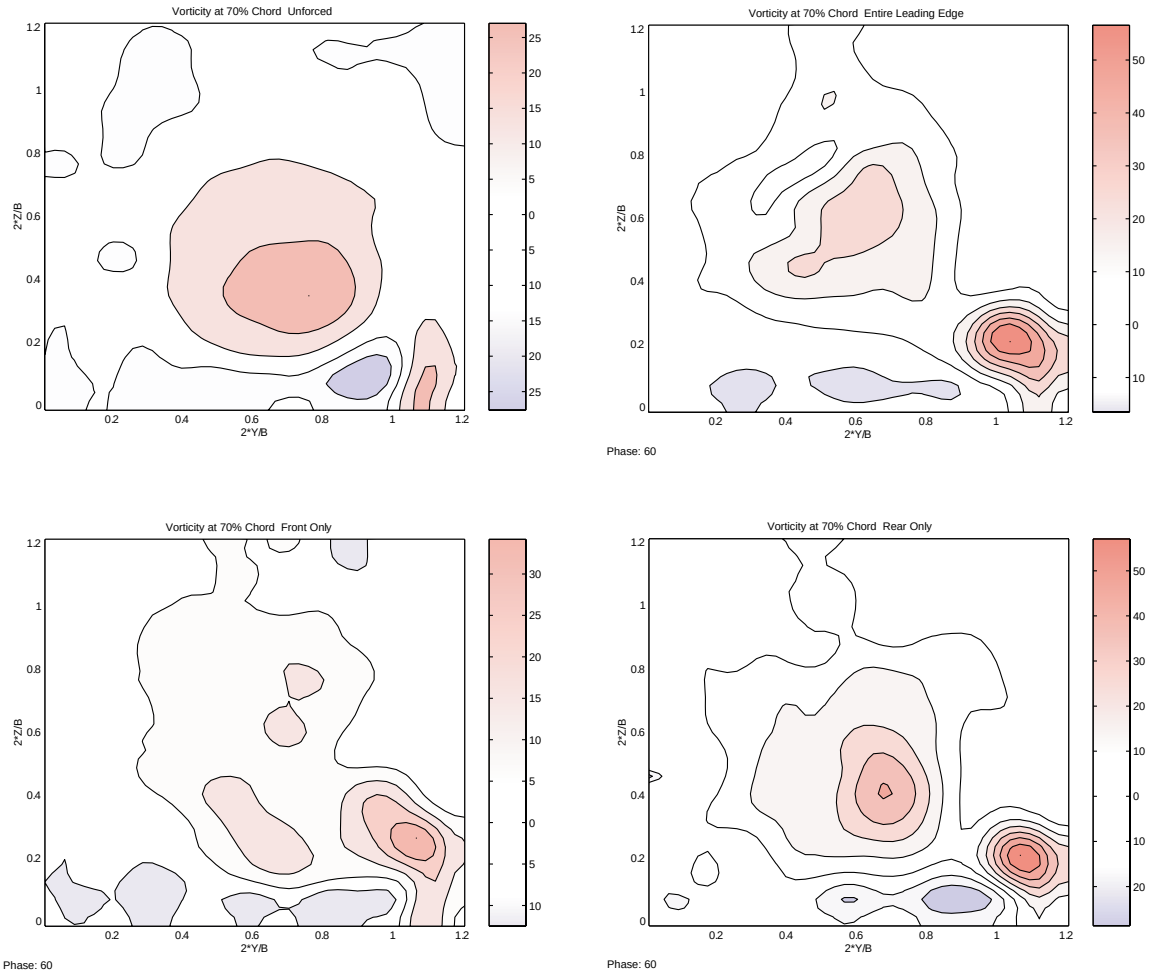

FIGURE 8. Vorticity at 70% of the root chord for the unforced, entire leading edge, front and rear only cases. All forced cases are shown at 60 degrees phase of the forcing cycle

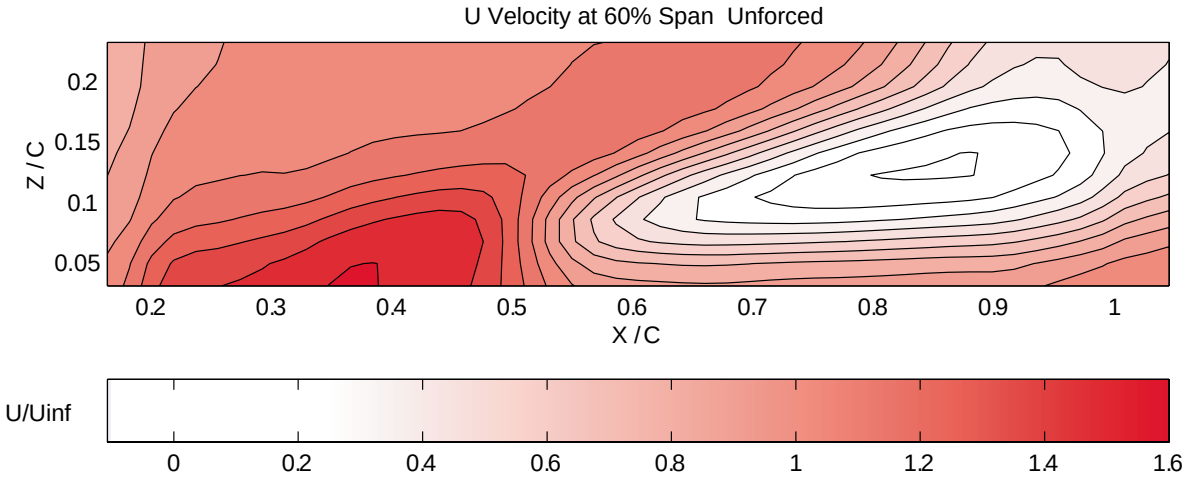

FIGURE 9. U Velocity 60% of the local wing span. Unforced Flow

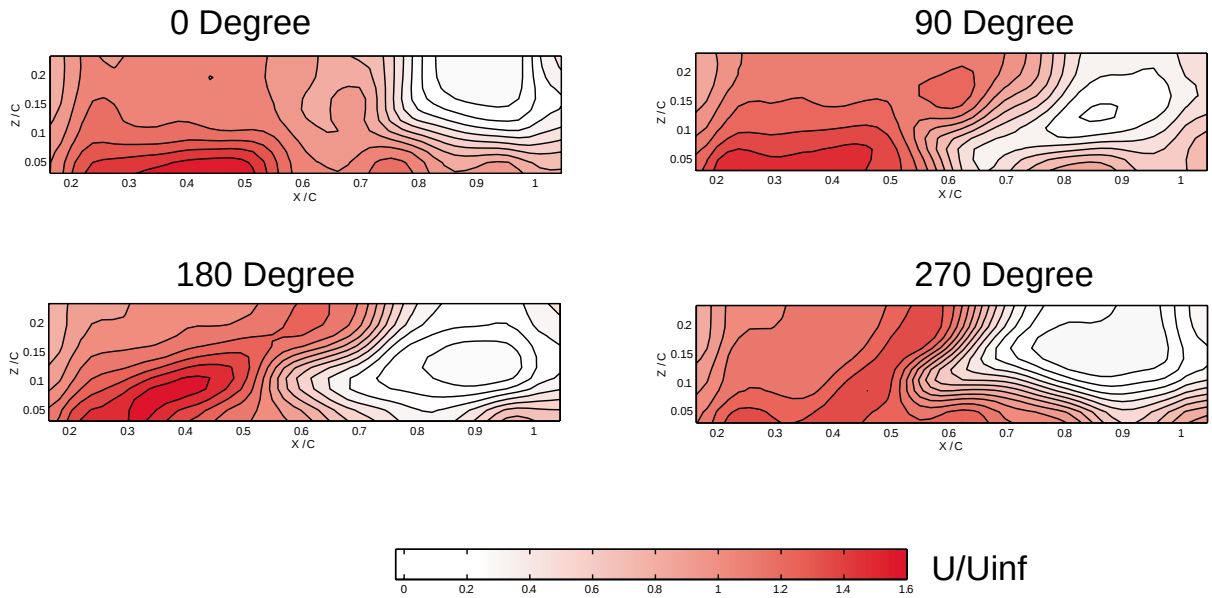

FIGURE 10. U Velocity at 60% of the local wing span. Flow forced from 20% to 100% of the chord ("Entire Leading Edge")

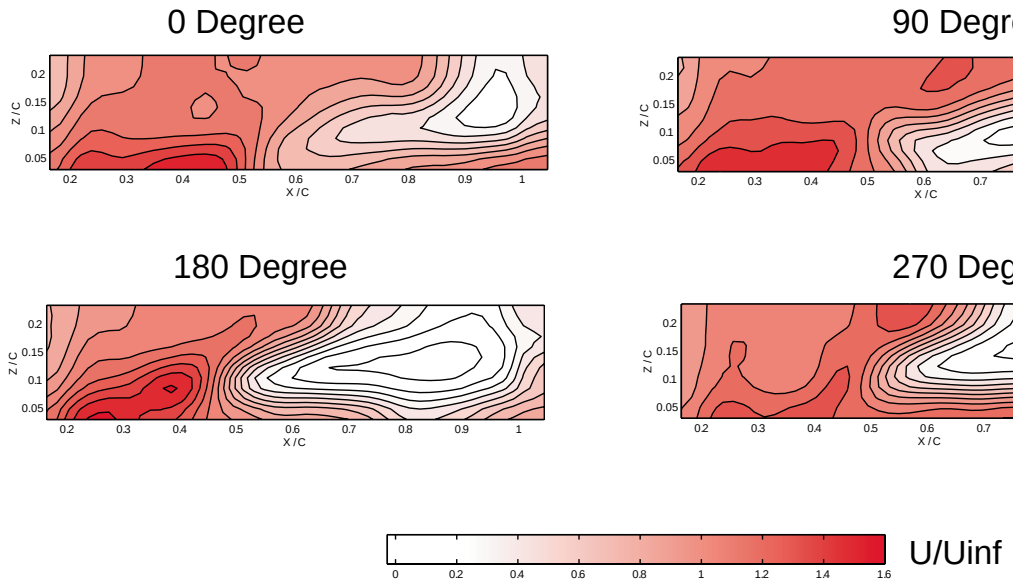

FIGURE 11. U Velocity at 60% of the local wing span. Flow forced from 20% to 50% of the chord ("Front")

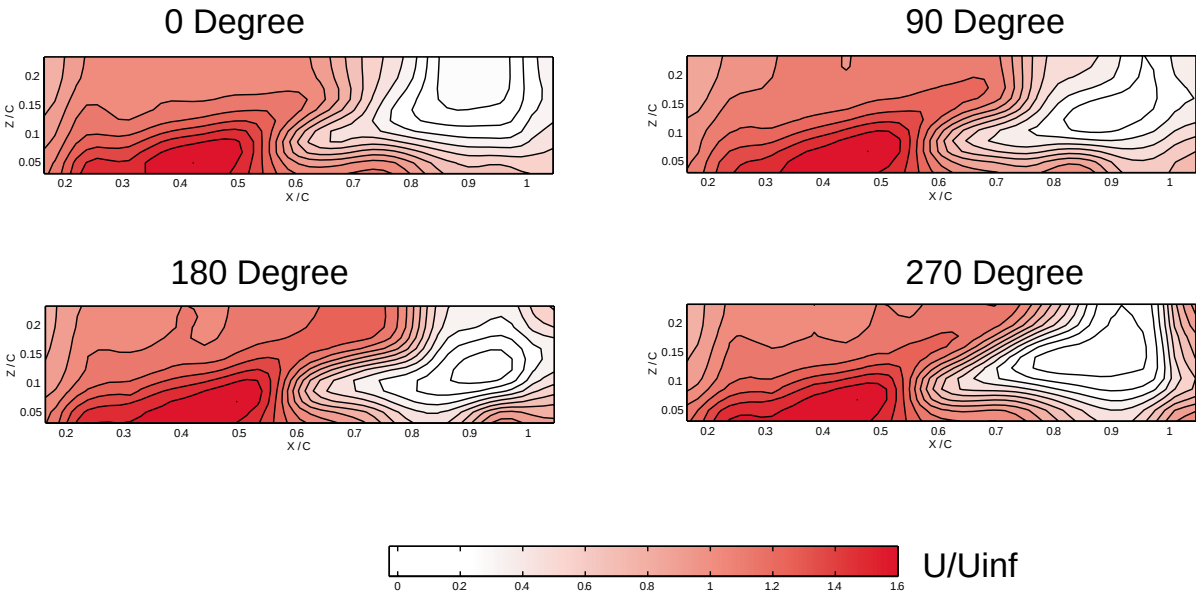

FIGURE 12. U Velocity at 60% of the local wing span. Flow forced from 60% to 100% of the chord ("Rear")

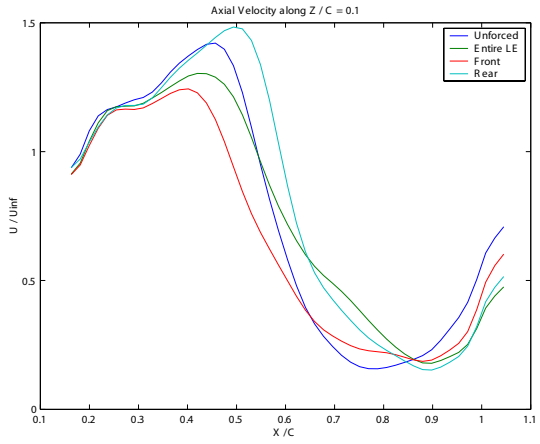

FIGURE 13. Axial Velocity at 60% Span, 10% of the root chord above the wing. The forced cases are averaged over all forcing phase angles.

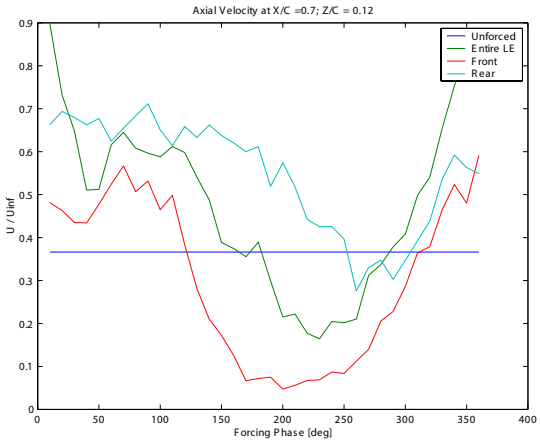

FIGURE 14. Axial Velocity at the location of X/C = 0.7, Y/C = 0.6 , Z/C = 0.12.

stationary. There is a secondary vortex of opposite sign above the surface near the leading edge.

With forcing along the entire leading edge, the vortex resulting from the instantaneous blowing can be seen near the wingtip. Interaction of this vortex causes the primary vortex to shift inboard and down at this phase angle. As Reference 1 showed, this movement over the forcing cycle causes the vortex center to trace out an ellipse, moving spanwise and wing normal. There was little effect on the peak vorticity relative to the unforced case.

Interestingly, front only forcing had a nearly identical effect as that on the entire leading edge. There are no significant differences in the primary or tip vortex peak vorticity, vortex locations, or movement pattern. Rear only forcing, on the other hand, produces a vorticity pat-

tern very similar to the unforced case, with little change of vorticity near the tip. This is to be expected, since in this case, the forcing is introduced well downstream of the 40% chord location.

Vorticity at the 70% chord location for the same phase angle and forcing conditions are shown in Figure 8. At this streamwise location the primary vortex has broken down in all cases. One may observe the forced tip vortex in the entire leading edge and rear only forcing cases. In the front only case, only a small amount of vorticity can be seen at the tip, convected downstream from the 20-60% chord forcing.

Based on the streamwise vorticity measured in the unforced case (Figure 7), a series of measurements evaluating the velocity component along the vortex core was conducted. For all of these measurments the laser light sheet was aligned normal to the wing at a constant 60% of the wing span, which coincides with the location of the vortex in the unforced case. Figure 9 shows the velocity component parallel to the wing for the unforced flow. It can be observed that the breakdown of the main vortex leaves a strong wake, starting between 50 and 60 percent of the root chord. This wake is responsible for the loss of lift experienced in the rear portion of the delta wing downstream of vortex breakdown. In the unforced flow field the axial velocity in the wake drops below 50 percent free stream velocity at about 55 percent of the chord.

Figure 10 shows the same region of the flow, but with forcing enabled from 20 to 100 percent of the chord. Four different phase angles, 0 degrees, which is at the start of the blowing cycle, 90 degrees, at the peak of the blowing cycle, 180 degrees, at the beginning of the suction cycle, and 270 degrees, at the peak of the suction cycle, are shown. The axial velocity shows a strong dependence on the phase of the forcing, with the largest changes visible during the blowing cycle. At the start of the blowing cyle, the wake has been pushed far downstream, the drop below 50 percent of the free stream velocity occurs at about 75 percent chord. During the blowing cycle the wake moves upstream to remain mostly stationary throughout the suction cycle around 60 percent of the chord. Averaged over the entire cycle there is an improvement in axial velocity, as compared to the unforced case. This explains the increase in normal force that was measured in the wind tunnel experiments using the entire leading edge for forcing.

Figure 11 shows the same axial velocity plots for the front forcing case. The front portion forcing shows little change throughout the forcing cycle with respect to the location where the velocity drops to less than 50 percent free stream velocity. At all phase angles this drop is located between 45 and 50 percent of the root chord, and thus occurs at about the same location as in the unforced case, if not further upstream. The size and strength of the wake region does however vary. Again the relative change in axial velocity as compared to the unforced case matches the finding of the wind tunnel force measurements, which show no significant increase in normal force for the front portion forcing setup.

The axial velocity for the rear portion forcing case is shown in Figure 12. Similar to the front portion forcing there is no great variablity throughout the forcing cycle. However, the axial velocity drop has moved downstream as compared to the unforced case, from around 55 percent chord to around 60 percent chord. This agrees with the wind tunnel force measurements, which found an increase in normal force for the rear portion forcing similar to the entire leading edge forcing setup.

Figure 13 compares the axial velocity profiles of all four cases, unforced, entire leading edge, front and rear portion with each other. The data is extracted at a constant distance of $Z / C = 0.1$ from the wing surface using the same data used for the contour plots shown in Figure 9 through Figure 12. For the forced cases the data was averaged over all forcing cycles, for the unforced cases it was averaged in time. The plot confirms the findings from the contour plots presented above in that it shows the velocity drop to occur furthest upstream for the front forcing case. Entire leadinge edge forcing and unforced cases follow, however in the entire leading edge forcing case a higher residual velocity is maintained after the drop occurs. The rear forcing case shows the velocity drop furthest downstream, while at the same time maintaining a residual velocity comparable to the entire leading edge forcing case. There is also a higher peak velocity upstream of the velocity drop associated with the rear forcing case as compared to the unforced case.

Figure 14 samples the axial velocity data sets at one spatial location, $Y/C = 0.6$ and $Z/C = 0.12$. This location was chosen well downstream of the vortex breakdown in the unforced case, in the center of the wake. Throughout the forcing cycle, the front portion forcing shows the largest fluctuations in axial velocity while averaging well below the unforced case. The entire leading edge forcing shows similarly large velocity fluctuations, but with an average above the unforced case. The rear forcing causes the smallest fluctuations in normal force but the highest overall average.

While the wind and water tunnel setups were different from each other in Reynolds number, their results complement each other well in shedding light on the mechanisms responsible for lift increase due to forcing. The findings agree well in a qualitative fashion even though they are not quantitatively comparable.

Conclusions

Forcing along portions of the leading edge was found to increase lift the most when applied towards the rear of the delta wing. Forcing along the front portion of the leading edge, upstream of vortex breakdown, did not significantly increase lift. That energy apparently went into altering the location of the primary vortex. PIV measurements showed any increase is due to the shear layer vortex caused by the forcing carrying high axial momentum fluid into the wake downstream of vortex breakdown. This increase in axial momentum decreased surface pressure and therfore increased normal force. The vortex breakdown location was not affected by the forcing.

Outlook

While all the blowing and suction slots were actuated in sync for the measurements presented, future research options include forcing with varying phase along the leading edge. This may create a curved main vortex which should be more resistant to breakdown. Since both wind and water tunnel measurements have their distinct limits, it would be very desirable to have CFD data to complement the results of this research.

Acknowledgements

The first author of this paper would like to acknowledge funding by the National Research Council in the form of a postdoctoral fellowship.

All authors would like to thank Dr. Yair Guy for kindly providing the wind tunnel data presented in this paper.

References

1. S.G. Siegel, T. E. McLaughlin, J.A. Morrow, 2001 "PIV Measurements on a Delta Wing with Periodic Blowing and Suction", AIAA 2001-2436

2. Guy, Y., Morrow, J. A., McLaughlin, T. E., "Control of Vortex Breakdown on a Delta Wing by Periodic Blowing and Suction", AIAA Paper 99-0132, 1999.

3. Guy, Y., Morrow, J. A., McLaughlin, T. E., and Wygnanski, I., "Pressure Measurements and Flow Field Visualization on a Delta Wing with Periodic Blowing and Suction ", AIAA Paper 99-4178, 1999.

4. Greenblat, D. and Wygnanski, I., "Dynamic Stall Control by Oscillatory Forcing", AIAA Paper 98-0676, 1998.

5. Nishri, B., "On the Dominant Mechanisms Governing Active Control of Separation", Ph.D. Thesis, Tel-Aviv University, Israel

6. Nishri, B. and Wygnanski, I., "On the Flow Separation and its Control", Computational Methods in Applied Science, 1996.

7. Seifert, A., Darabi, A. and Wygnanski, I., "Delay of Airfoil Stall by Periodic Excitation", AIAA Journal of Aircraft, Vol. 33, No. 4, 1996.

8. Nave, T., "The Effect of Sweep on Separation Control over an Airfoil", M.Sc. Thesis, Tel-Aviv University, Israel, 1997.

9. Seifert, A., Darabi, A. and Wygnanski, I., "The Effects of Forced Oscillations on the Performance of Airfoils", AIAA Paper 93-3264, 1993.

10. Wygnanski, I. and Seifert, A., "The Control of Separation by Periodic Oscillations", AIAA Paper 94-2608, 1994.

11. Guy, Y., Morrow, J. A., McLaughlin, T. E., and Wygnanski, I., "Velocity Measurements on a Delta Wing with Periodic Blowing and Suction ", AIAA Paper 00-0550, 2000.

12. Guy, Y., Morton, S.A., Morrow, J. A., "Numerical Investigation of the Flow Field on a Delta Wing with Periodic Blowing and Suction", AIAA 2000-2321, 2000.